The scattering of electromagnetic radiation from finite dielectric circular cylinders

1983 J. Phys. A: Math. Gen. 16 651

(http://iopscience.iop.org/0305-4470/16/3/024)

J. Phys. A: Math. Gen. **16** (1983) 651–662. Printed in Great Britain

The scattering of electromagnetic radiation from finite dielectric circular cylinders

J W Shepherd and A R Holt

Department of Mathematics, University of Essex, Wivenhoe Park, Colchester CO4 3SQ, UK

Received 2 August 1982, in final form 14 September 1982

Abstract. The Fredholm integral equation method is applied to the scattering of electromagnetic waves by finite dielectric cylinders of circular cross section. The method is applied to a wide range of diameter/length ratios, including both rods and discs. Generally good agreement has been obtained with the experimental backscatter measurements of McCormick and Hendry.

1. Introduction

In previous papers (Uzunoglu and Holt 1977, Holt *et al* 1978, Holt 1980) we have described the application of the Fredholm integral equation method (FIM) to the problem of scattering of electromagnetic radiation from dielectric scatterers. The scatterers considered were either two dimensional (infinite cylinders of elliptic cross section) or three dimensional (spheroids and ellipsoids).

The problem had been generated from a need to have reliable estimates of attenuation and cross-polarisation for microwave propagation paths; oblate spheroids are reasonable models of raindrops. However, on earth–satellite links, ice has been shown to be a significant depolarising medium, even though it gives rise to little attenuation (for a review see Bostian and Allnutt 1979). Ice occurs in a number of different forms and shapes. In hail the particles are often large and the shape variable (Barge and Isaacs 1973). At high altitudes the particles can be either conglomerates or hexagonal crystals (Mason 1971, Ono 1970, Varley 1978). The crystals are often in the shape of plates or needles. In an effort to investigate the importance of shape in the scattering of electromagnetic waves in the microwave and millimetre wave bands, we have extended our application of the FIM.

In this work we have studied finite cylinders as a step towards modelling the discs and needles which arise in high-altitude ice.

There seem to be very few previous calculations for finite cylinders. Uzunoglu *et al* (1978) considered thin rods, Weil and Chu (1976, 1980) have considered thin discs and Morgan and Mei (1979) have reported one sample calculation. There is experimental evidence available: Allan and McCormick (1980a, b) have studied backscattering from a number of different shapes of circular cylinder, and have presented data on cross sections and on the amplitude and phase of the depolarisation. Their measurements may be regarded as very reliable, since their measurements of the same quantities for spheroids have been shown to agree excellently with theory (Holt 1982a)

and several different theoretical methods for spheroids are known to agree (cf Holt 1982b).

In § 2 we briefly describe the FIM. In § 3 we give details of the matrix element calculations for finite circular cylinders. In § 4 we give sample results and compare these results with the other available results, both theoretical and experimental.

2. Fredholm integral equation method

The method was first introduced by Holt and Santoso (1973) to study quantum scattering by a central potential, and was then extended to electromagnetic wave scattering by Uzunoglu *et al* (1976). An observation by Uzunoglu led to a modification involving a Fourier expansion. This modification has greatly improved the application, and has been described in detail by Holt (1980). It is this description that we summarise.

We consider a plane electromagnetic wave of wavevector $\boldsymbol{k}_0$ and polarisation vector $\hat{\boldsymbol{e}}_i$ incident on an axially symmetric dielectric scatterer of refractive index $n_0(\boldsymbol{r})$ and volume V. The dyadic integral equation describing this (with $\exp(-i\omega t)$ time dependence suppressed) is

$$\mathbb{E}(\boldsymbol{r}) = \mathbb{J}_0 \exp(i\boldsymbol{k}_0 \cdot \boldsymbol{r}) + \int_V \mathbb{G}(\boldsymbol{r}, \boldsymbol{r}')\gamma(\boldsymbol{r}')\mathbb{E}(\boldsymbol{r}')\, d\boldsymbol{r}' \tag{1}$$

where

$$\gamma(\boldsymbol{r}) = k_0^2(n_0^2(\boldsymbol{r}) - 1) \equiv k_0^2(\varepsilon(\boldsymbol{r}) - 1) \tag{2}$$

and, for any λ,

$$\mathbb{J}_\lambda = \mathbb{1} - \hat{\boldsymbol{k}}_\lambda \hat{\boldsymbol{k}}_\lambda. \tag{3}$$

The scattering amplitude tensor for scattering in the direction $\hat{\boldsymbol{k}}_s$ is

$$f = \frac{1}{4\pi}\mathbb{J}_s \cdot \int_V \exp(-i\boldsymbol{k}_s \cdot \boldsymbol{r})\gamma(\boldsymbol{r})\mathbb{E}(\boldsymbol{r})\, d\boldsymbol{r} \tag{4}$$

and thus the vector scattering amplitude for polarisation $\hat{\boldsymbol{e}}_i$ is

$$\boldsymbol{f} = \boldsymbol{f} \cdot \hat{\boldsymbol{e}}_i. \tag{5}$$

We can see from (4) that a knowledge of the field inside the scatterer is sufficient to determine the scattering. If we premultiply (1) by $\exp(-i\boldsymbol{k}_1 \cdot \boldsymbol{r})\gamma(\boldsymbol{r})$, where $\boldsymbol{k}_1$ is for the present arbitrary, and integrate throughout the scatterer, we then have an integral equation which involves only the interior field. Formally we have

$$\langle \boldsymbol{k}_1|\gamma|\mathbb{E}\rangle = \langle \boldsymbol{k}_1|\gamma|\mathbb{E}_0\rangle + \langle \boldsymbol{k}_1|\gamma\mathbb{G}\gamma|\mathbb{E}\rangle. \tag{6}$$

We have lost all information on the exterior field, though it may be regained from (1). The interior field is Fourier transformable, and we write

$$\mathbb{E}_{int}(\boldsymbol{r}) = \int \mathbb{C}(\boldsymbol{k}_2, \boldsymbol{k}_0) \exp(i\boldsymbol{k}_2 \cdot \boldsymbol{r})\, d\boldsymbol{k}_2. \tag{7}$$

Substituting (7) into (6) and (4) gives

$$\int d\boldsymbol{k}_2\, \mathbb{K}(\boldsymbol{k}_1, \boldsymbol{k}_2)\mathbb{C}(\boldsymbol{k}_2, \boldsymbol{k}_0) = \mathbb{J}_0 U(\boldsymbol{k}_1, \boldsymbol{k}_0) \tag{8}$$

and

$$f(\boldsymbol{k}_s, \boldsymbol{k}_0) = \frac{1}{4\pi} \mathbb{J}_s \int \mathrm{d}\boldsymbol{k}_2 \, \mathbb{C}(\boldsymbol{k}_2, \boldsymbol{k}_0) U(\boldsymbol{k}_s, \boldsymbol{k}_2) \tag{9}$$

where

$$U(\boldsymbol{k}_1, \boldsymbol{k}_2) = \langle \boldsymbol{k}_1 | \gamma | \boldsymbol{k}_2 \rangle \tag{10}$$

and

$$\mathbb{K}(\boldsymbol{k}_1, \boldsymbol{k}_2) \doteq \langle \boldsymbol{k}_1 | \gamma \mathbb{1} - \gamma \mathbb{G} \gamma | \boldsymbol{k}_2 \rangle. \tag{11}$$

Equations (8) and (9) may be solved by reducing the integrations by numerical quadrature, thus obtaining a matrix equation from which f may be obtained. This has been shown to be numerically stable since the amplitude so obtained satisfies the Schwinger variational principle (Holt *et al* 1978).

For incident polarisation $\hat{\boldsymbol{e}}_i$, we take the (post) scalar product obtaining

$$\int \mathrm{d}\boldsymbol{k}_2 \, \mathbb{K}(\boldsymbol{k}_1, \boldsymbol{k}_2) \boldsymbol{c}(\boldsymbol{k}_2, \boldsymbol{k}_0) = \hat{\boldsymbol{e}}_i U(\boldsymbol{k}_1, \boldsymbol{k}_0) \tag{12}$$

and

$$f(\boldsymbol{k}_s, \boldsymbol{k}_0) = \frac{1}{4\pi} \mathbb{J}_s \cdot \int \mathrm{d}\boldsymbol{k}_2 U(\boldsymbol{k}_s, \boldsymbol{k}_2) \boldsymbol{c}(\boldsymbol{k}_2, \boldsymbol{k}_0). \tag{13}$$

For homogeneous scatterers, only one wave number occurs in (7) (cf Devaney and Wolf 1974). We expand the azimuthal dependence in a Fourier series, and we describe the field in terms of the components $(1/\sqrt{2})(E_x \pm \mathrm{i}E_y), E_z$. Thus

$$\boldsymbol{c}(\boldsymbol{k}_2, \boldsymbol{k}_0) = \delta(k_2 - k_0 n_0) \boldsymbol{T} \boldsymbol{d} \tag{14}$$

where

$$T = \frac{1}{\sqrt{2}} \begin{pmatrix} 1 & 1 & 0 \\ -i & i & 0 \\ 0 & 0 & \sqrt{2} \end{pmatrix} \tag{15}$$

and

$$\boldsymbol{d}(\hat{\boldsymbol{k}}_2, \boldsymbol{k}_0) = \sum_{s=-S}^{+S} \boldsymbol{d}_s(x_2) \exp(s\mathrm{i}\varphi_2) \tag{16}$$

$(x_2 = \cos\theta_2)$.

For a general axially symmetric body it has been shown (Shepherd 1981) that the matrix equation resulting from applying quadrature to (8) is in block diagonal form, each block being

$$\begin{pmatrix} L_{11}^{r+2} & L_{12}^{r+2} & L_{13}^{r+2} \\ (L_{12}^{r+2})^{\mathrm{T}} & L_{11}^{r} & (L_{13}^{r+1})^{\mathrm{T}} \\ (L_{13}^{r+2})^{\mathrm{T}} & L_{13}^{r+1} & L_{33}^{r+1} \end{pmatrix} \begin{pmatrix} d_{1,r+2} \\ d_{2,r} \\ d_{3,r+1} \end{pmatrix} = \begin{pmatrix} U_{r+2} h_1 \\ U_r h_2 \\ U_{r+1} h_3 \end{pmatrix} \tag{17}$$

where

$$\boldsymbol{d}_r = (d_{1,r}, d_{2,r}, d_{3,r})^{\mathrm{T}} \tag{18}$$

and

$$U_r = \int_0^{2\pi} d\varphi_2 \exp(-ir\varphi_2) U(\boldsymbol{k}_2, \boldsymbol{k}_0). \tag{19}$$

Each L partition in (17) is of dimension N, where N is the number of pivots in the numerical quadrature. Details of the matrix element evaluation for spheroids have been given by Holt (1980). We describe the evaluation of the matrix elements for circular cylinders in § 3.

One point which should be mentioned concerns the edges, since this is a problem in methods, such as the T matrix method (cf Waterman 1969), which involves surface currents. As far as the internal field is concerned the important point is that in the neighbourhood of an edge the 'energy finiteness condition' (Jones 1964) should be satisfied. This is guaranteed in the FIM since the internal field is assumed to be Fourier transformable.

3. Matrix elements for finite circular cylinders

The heart of the calculation lies in the evaluation of the matrix elements $U(\boldsymbol{k}_1, \boldsymbol{k}_2)$ and $\mathbb{K}(\boldsymbol{k}_1, \boldsymbol{k}_2)$. In the evaluation of the latter, the singularity inherent in the original integral equation (1) is integrated out analytically, resulting in a non-singular kernel $\mathbb{K}$.

The calculation of

$$U(\boldsymbol{k}_1, \boldsymbol{k}_2) = \int_V \exp[-i(\boldsymbol{k}_1 - \boldsymbol{k}_2)\cdot \boldsymbol{r}]\gamma(\boldsymbol{r})\, d\boldsymbol{r} \tag{20}$$

is straightforward when the scatterer is homogeneous, i.e. when $\gamma(\boldsymbol{r}) = \gamma$. If the cylinder has radius a and height $2b$, and if we describe $\boldsymbol{k}_1, \boldsymbol{k}_2$ in cylindrical coordinates ($\boldsymbol{k}_1 = (k_{1\rho}, \varphi_1, k_{1z})$), then we find

$$U(\boldsymbol{k}_1, \boldsymbol{k}_2) = 4\pi a^2 b\gamma \frac{J_1(aR)}{aR} j_0(bz_{12}) \tag{21}$$

where

$$z_{12} = k_{1z} - k_{2z} \tag{22}$$

and

$$R^2 = k_{1\rho}^2 + k_{2\rho}^2 - 2k_{1\rho}k_{2\rho}\cos(\varphi_1 - \varphi_2). \tag{23}$$

In equation (21), $j_0(x)$ is the zeroth-order spherical Bessel function, and $J_1(x)$ is the first-order Bessel function. To obtain U_r (equation (19)) we use the expansion (Watson 1966)

$$\frac{J_\nu(a|\boldsymbol{r} - \boldsymbol{r}'|)}{|\boldsymbol{r} - \boldsymbol{r}'|^\nu} = 2^\nu \Gamma(\nu) \sum_{m=0}^{\infty} (m + \nu) \frac{J_{\nu+m}(ar)}{r^\nu} \frac{J_{\nu+m}(ar')}{r'^\nu} C_m^\nu(\hat{\boldsymbol{r}}\cdot\hat{\boldsymbol{r}}') \tag{24}$$

where C_m^ν is the Gegenbauer polynomial.

Using the relation

$$\int_0^{2\pi} d\varphi \exp(ir\varphi) C_m^1(\cos(\varphi - \varphi_2)) = \begin{cases} 2\pi \exp(ir\varphi_2) & r + m \text{ even}, |r| \leqslant m \\ 0 & \text{otherwise} \end{cases} \tag{25}$$

we obtain

$$U_r = 16\pi^2\gamma \exp(-\mathrm{i}r\varphi_2) j_0(bz_{12}) \sum_{\substack{t=|r| \\ t+r \text{ even}}}^{\infty} (t+r) \frac{J_{t+1}(ak_{1\rho})}{k_{1\rho}} \frac{J_{t+1}(ak_{2\rho})}{k_{2\rho}}. \tag{26}$$

As shown by Holt *et al* (1978),

$$\mathbb{K}(\boldsymbol{k}_1, \boldsymbol{k}_2) = \mathbb{1}n_0^2 U(\boldsymbol{k}_1, \boldsymbol{k}_2) - \mathbb{Z}(\boldsymbol{k}_1, \boldsymbol{k}_2) \tag{27}$$

where

$$\mathbb{Z}(\boldsymbol{k}_1, \boldsymbol{k}_2) = \frac{1}{8\pi^3 k_0^2} \lim_{\varepsilon \to 0^+} \int \frac{p^2 \, \mathrm{d}\boldsymbol{p}}{p^2 - k_0^2 - \mathrm{i}\varepsilon} (\mathbb{1} - \hat{p}\hat{p}) U(\boldsymbol{k}_1, \boldsymbol{p}) U(\boldsymbol{p}, \boldsymbol{k}_2). \tag{28}$$

We need to calculate

$$\mathbb{Y}_{rs} = \int_0^{2\pi} \mathrm{d}\varphi_1 \exp(-\mathrm{i}r\varphi_1) \int_0^{2\pi} \mathrm{d}\varphi_2 \exp(\mathrm{i}s\varphi_2) T^{-1} \mathbb{Z}(\boldsymbol{k}_1, \boldsymbol{k}_2) T \tag{29}$$

where T is given in (15). Using (26) we find

$$\begin{aligned} \mathbb{Y}_{rs} = \frac{64a^4b^2\gamma^2\pi^2}{k_0^2} & \sum_{\substack{t=|r| \\ t+r \text{ even}}}^{\infty} \sum_{\substack{u=|s| \\ u+s \text{ even}}}^{\infty} (u+1)(t+1) \frac{J_{t+1}(ak_{1\rho}) J_{t+1}(ak_{2\rho})}{(ak_{1\rho})(ak_{2\rho})} \\ & \times \int_{-\infty}^{+\infty} \mathrm{d}z \int_0^{\infty} \frac{\rho \, \mathrm{d}\rho}{\rho^2 + z^2 - k_0^2} j_0[b(z - k_{1z})] j_0[b(z - k_{2z})] \frac{J_{t+1}(a\rho) J_{u+1}(a\rho)}{\rho^2} \\ & \times \begin{pmatrix} (z^2 + \frac{1}{2}\rho^2)\delta_{r,s} & -\frac{1}{2}\rho^2\delta_{r,s+2} & -(\rho z/\sqrt{2})\delta_{r,s+1} \\ -\frac{1}{2}\rho^2\delta_{r+2,s} & (z^2 + \frac{1}{2}\rho^2)\delta_{r,s} & -(\rho z/\sqrt{2})\delta_{r+1,s} \\ -(\rho z/\sqrt{2})\delta_{r+1,s} & -(\rho z/\sqrt{2})\delta_{r,s+1} & \rho^2\delta_{r,s} \end{pmatrix}. \end{aligned} \tag{30}$$

To evaluate the integrals in (30) we use the expansion

$$j_0[b(x-y)] = \sum_{n=0}^{\infty} (2n+1) j_n(bx) j_n(by). \tag{31}$$

This has the advantage that the integrals are decoupled from the components of $\boldsymbol{k}_1, \boldsymbol{k}_2$. Thus one evaluation of the integrals suffices for calculating all the matrix elements. We finally obtain, on performing the z integration,

$$\begin{aligned} & \mathbb{Y}_{rs}(k_{1z}, k_{1\rho}, k_{2z}, k_{2\rho}) \\ & = \frac{32a^4b^2\gamma^2\pi^3\mathrm{i}}{k_0^2} \sum_{m=0}^{\infty} \sum_{n=0}^{\infty} \sum_{\substack{t=|r| \\ t+r \text{ even}}}^{\infty} \sum_{\substack{u=|s| \\ u+s \text{ even}}}^{\infty} (2m+1)(2n+1)(t+1)(u+1) \\ & \quad \times \frac{J_{t+1}(ak_{1\rho})}{ak_{1\rho}} \frac{J_{u+1}(ak_{2\rho})}{ak_{2\rho}} j_n(bk_{1z}) j_m(bk_{2z}) \\ & \quad \times \begin{pmatrix} (I_2 + \frac{1}{2}I_1)\delta_{r,s} & -\frac{1}{2}I_1\delta_{r,s+2} & -(1/\sqrt{2})I_3\delta_{r,s+1} \\ -\frac{1}{2}I_1\delta_{r+2,s} & (I_2 + \frac{1}{2}I_1)\delta_{r,s} & -(1/\sqrt{2})I_3\delta_{r+1,s} \\ -(1/\sqrt{2})I_3\delta_{r+1,s} & -(1/\sqrt{2})I_3\delta_{r,s+1} & I_1\delta_{r,s} \end{pmatrix} \end{aligned} \tag{32}$$

where

$$I_1(m, n, t, u) = \tfrac{1}{2}[1+(-1)^{m+n}] \int_0^\infty \frac{\rho}{\tau} \mathrm{d}\rho J_t(a\rho) J_u(a\rho) \left(j_{m_>}(b\tau) h^{(1)}_{m_<}(b\tau) + \frac{\mathrm{i}\delta_{mn}}{(2m+1)b\tau} \right) \tag{33}$$

$$I_2(m, n, t, u) = \tfrac{1}{2}[1+(-1)^{m+n}] \int_0^\infty \frac{\tau}{\rho} \mathrm{d}\rho\, J_t(a\rho) J_u(a\rho)\, j_{m_>}(b\tau) h^{(1)}_{m_<}(b\tau) \tag{34}$$

$$I_3(m, n, t, u) = \tfrac{1}{2}[1-(-1)^{m+n}] \int_0^\infty \mathrm{d}\rho\, J_t(a\rho) J_u(a\rho) j_{m_>}(b\tau) h^{(1)}_{m_<}(b\tau) \tag{35}$$

where

$$m_{<,>} = \min, \max(m, n) \tag{36}$$

and

$$\tau = (k_0^2 - \rho^2)^{1/2}. \tag{37}$$

The integrals in (33)–(35) have been performed numerically. It should be noted that they are independent of the refractive index. Details of the numerical procedures used have been given by Shepherd (1981).

4. Results

The essential part of any research which involves heavy computation is adequate checking with independent research. Our first check has been with the work of Uzunoglu *et al* (1978). In table 1 we compare our scattering amplitudes with the results they obtained for a thin cylinder. It will be seen that the real parts are in excellent agreement, whereas the imaginary parts differ by around 50%. We believe the reason for this lies in the nature of the approximation made by Uzunoglu *et al.* Their assumptions were similar to those of Rayleigh theory. The latter also estimates the imaginary part of the scattering amplitudes less accurately than it does the real part (see, e.g., Shepherd (1981), and table 2 below).

Our next checks are with the observations of Allan and McCormick (1980a, b). They have performed experiments on a number of sample shapes of synthetic ice, measuring the backscattered power and cross-polarisation. In figures 1–6 we compare our results with theirs for several samples, ranging in axial ratio from 'rod' to 'discs'. The quantities being compared are σ, ν and δ where

$$\sigma = |f_V(\pi) + f_H(\pi)|^2 / 4\pi \tag{38}$$

$$\nu \exp(\mathrm{i}\delta) = \beta \frac{f_H(\pi) - f_V(\pi)}{f_H(\pi) + f_V(\pi)} \tag{39}$$

with $\beta = +1$ for discs and (-1) for rods.

Table 1. Forward scattering amplitude for scattering of vertically polarised radiation incident perpendicular to the axis of a thin rod of refractive index 1.4.

k_0a	c/a	This work	Uzunoglu *et al* (1978)
0.02	12.5	4.66(−5)+i1.44(−9)	4.67(−5)+i2.28(−9)

Table 2. Forward and backward scattering amplitudes for a disc of axial ratio 64 : 1, $n_0 = 1.78 + i0.0024$, $k_0 a = 0.84$.

Direction	f_0	f_V	f_H	Shape
Forward	$1.56\times10^{-3}+i1.23\times10^{-5}$	$5.10\times10^{-4}+i1.21\times10^{-6}$	$1.56\times10^{-3}+i1.15\times10^{-5}$	Spheroid (exact)
	$1.55\times10^{-3}+i5.93\times10^{-6}$	$5.09\times10^{-4}+i6.43\times10^{-7}$	$1.55\times10^{-3}+i5.93\times10^{-6}$	Spheroid (Rayleigh)
	$1.52\times10^{-3}+i1.17\times10^{-5}$	$5.15\times10^{-4}+i1.26\times10^{-6}$	$1.54\times10^{-3}+i1.11\times10^{-5}$	Cylinder
Backward	$1.56\times10^{-3}+i1.23\times10^{-5}$	$3.80\times10^{-4}+i1.04\times10^{-6}$	$1.16\times10^{-3}+i9.91\times10^{-6}$	Spheroid (exact)
	$1.55\times10^{-3}+i5.93\times10^{-6}$	$5.09\times10^{-4}+i6.43\times10^{-7}$	$1.55\times10^{-3}+i5.93\times10^{-6}$	Spheroid (Rayleigh)
	$1.52\times10^{-3}+i1.17\times10^{-5}$	$3.94\times10^{-4}+i1.10\times10^{-6}$	$1.12\times10^{-3}+i9.28\times10^{-6}$	Cylinder

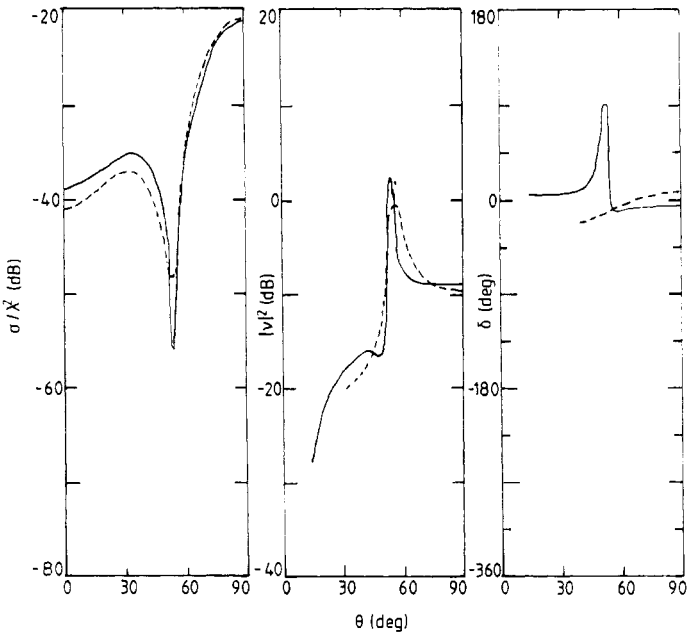

Figure 1. Backscattering by rod scatterer with $ka = 0.267$, $c/a = 9.99$, $\varepsilon = 3.15 - i0.036$. —— theory; ----- expt.

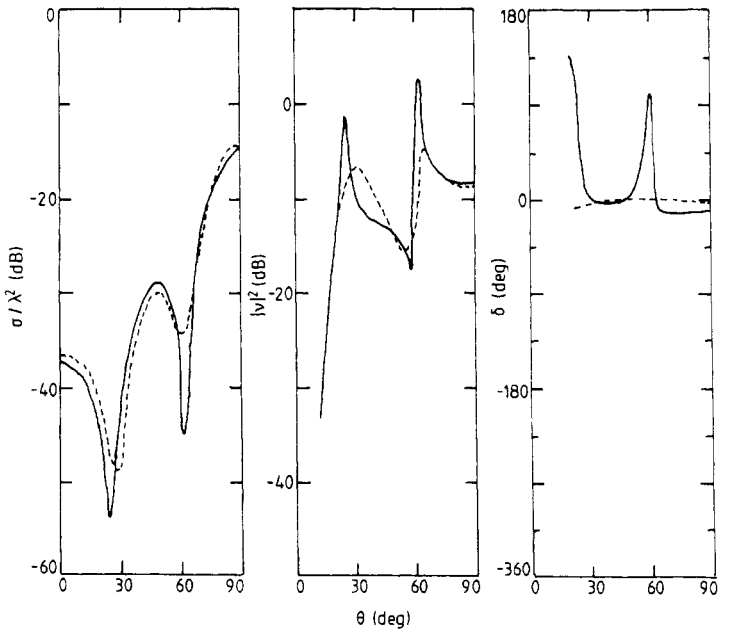

Figure 2. Backscattering by rod scatterer with $ka = 0.343$, $c/a = 10.00$, $\varepsilon = 3.14 - i0.036$. —— theory; ----- expt.

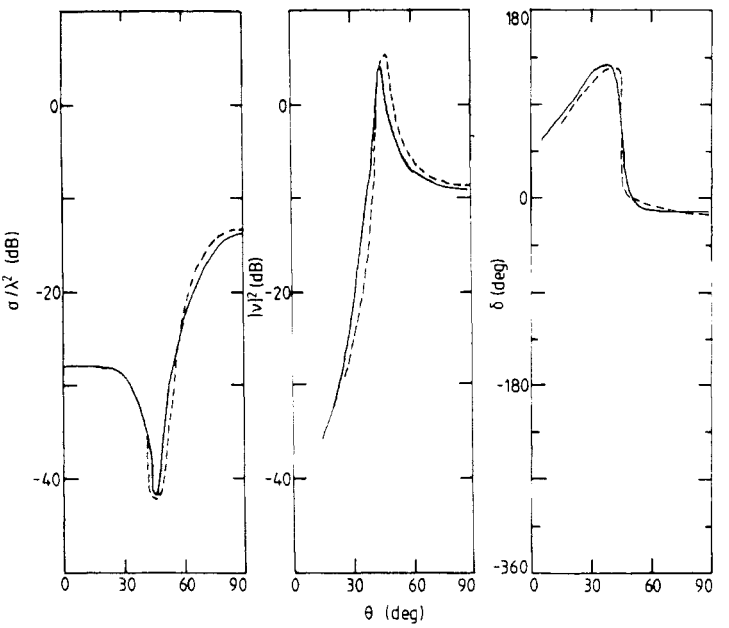

Figure 3. Backscattering by rod scatterer with $ka = 0.458$, $c/a = 5.00$, $\varepsilon = 3.14 - i0.036$
—— theory; ----- expt.

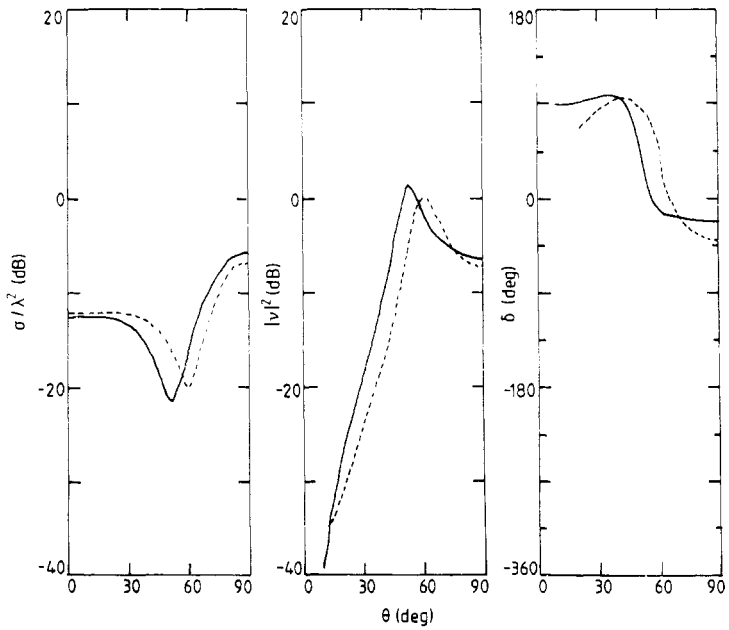

Figure 4. Backscattering by rod scatterer with $ka = 0.914$, $c/a = 2.498$, $\varepsilon = 3.14 - i0.036$.
—— theory; ----- expt.

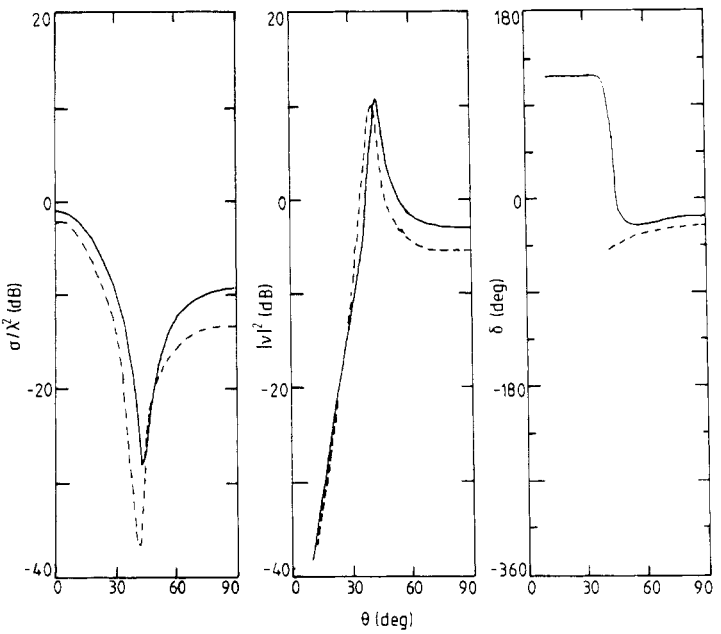

Figure 5. Backscattering by disc scatterer with $ka = 2.285$, $c/a = 0.2013$, $\varepsilon = 3.12 - i0.036$. —— theory; ----- expt.

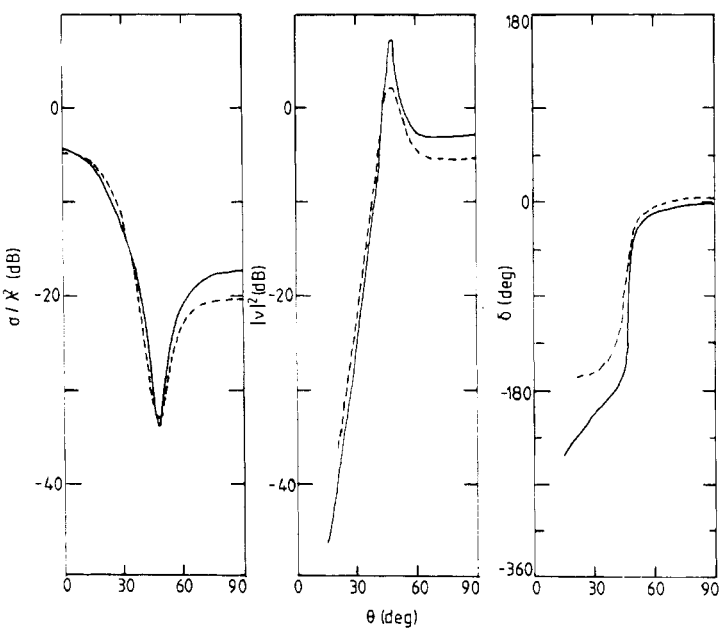

Figure 6. Backscattering by disc scatterer with $ka = 2.283$, $c/a = 0.1008$, $\varepsilon = 3.13 - i0.036$. —— theory; ----- expt.

$f_{V,H}(\pi)$ are the backscattering amplitudes for vertically or horizontally polarised incident radiation. It should be noted that the theory and experiment assumed opposite signs in the time dependence (and hence used opposite signs for the imaginary part of the refractive index). This results in opposite signs for δ. However, to make a comparison, we have adopted the sign convention of Allan and McCormick, both for δ and the quoted value of the complex permittivity ε.

A backscatter comparison is always a more sensitive test than a forward-scatter comparison, since the various partial waves give contributions whose signs alternate, whereas for forward scattering they all have the same sign. The agreement between theory and experiment is seen to be satisfactory. In figures 1 and 2 we plot σ/λ^2, $|\nu|^2$ and δ for rods of axial ratio 10 : 1 and two different sizes. We note that the curves for σ/λ^2 and $|\nu|^2$ are in broad agreement, though the theory tends to accentuate the peaks. We find peaks in δ which the experimental results do not reflect. In figures 3 and 4 we give results for rods of axial ratio 5 : 1 and 2.5 : 1 respectively. Again there is a good measure of agreement, except that the theoretical and experimental curves seem to be displaced in angle. In figures 5 and 6 we give results for discs of axial ratios 5 : 1 and 10 : 1 respectively. In both these cases agreement is least good when the incident radiation is orientated at approximately 90° to the axis of the disc—i.e. it is incident on an edge of the discs. In making these comparisons we have used the parameters given by McCormick and Hendry. However, the backscatter amplitudes can be sensitive to these parameters, and this could be a cause of error. A second cause of error can result from the nature of the experiment. The samples were rotated at an even speed, and the quantities measured were obtained by fitting a good number of data points. In their paper McCormick and Hendry indicated that with some of their larger, more elongated samples, they had difficulty in maintaining a steady angle of rotation. Also it should be noted that there must inevitably be difficulty in measuring cross sections over a range of 35 dB. All these factors suggest that the theoretical results are in very good agreement with the experimental results over a wide range of axial ratio.

A final check is to compare the results for small cylinders with those for spheroids of the same volume and same axial ratio. In table 2 we give forward and backward scattering amplitudes for incidence along the axis of symmetry (f_0), and for both polarisations incident perpendicular to the axis of symmetry (f_V, f_H). The scatterer is a 'disc' of axis ratio 64 : 1. We also give for comparison the Rayleigh approximation for the spheroid, and note that this demonstrates our earlier comment.

The current implementation clearly has its limitations since, as the size parameter increases, so does the number of terms which need to be included in the summations in equation (32). In turn this means that the number of integrals to be calculated escalates rapidly. We believe that currently we can perform calculations for ice ($n_0 = 1.78 + \mathrm{i}\,0.0024$) for $k_0 d \leqslant 3.5$, where $d = \max(a, b)$.

5. Conclusion

We have extended the Fredholm integral equation method to scattering by finite circular cylinders and shown that our results are in good agreement with other available results. Using this method it will now be possible, for example, to examine the importance of shape in the study of cross-polarisation effects in the propagation of microwaves through tropospheric ice particles.

Acknowledgments

This work has been supported by the Science and Engineering Research Council through research grant number GR/B03207. All the calculations have been performed on the PDP-10 installation at the University of Essex. The help of the computer staff is gratefully acknowledged.

References

Allan L E and McCormick G C 1980a *National Research Council, Ottawa, Report ERB*-921
——1980b *IEEE Trans. Antennas Propag.* **AP-28** 166–9
Barge B L and Isaacs G A 1973 *J. Rech. Atmos.* **7** 11–20
Bostian C W and Allnutt J E 1979 *Proc. IEE* **126** 951–60
Devaney A J and Wolf E 1974 *J. Math. Phys.* **75** 234–44
Holt A R 1980 *Acoustic, Electromagnetic and Elastic Wave Scattering: Focus on the T-matrix approach* ed Varadan V V and V K (New York: Pergamon) pp 255–68
——1982a *IEE Trans. Antennas Propag.* **AP-30**
——1982b *Radio Science* **17** 929–45
Holt A R and Santoso B 1973 *J. Phys. B: At. Mol. Phys.* **6** 2010–7
Holt A R, Uzunoglu N K and Evans B G 1978 *IEE Trans Antennas Propag.* **AP-26** 706–12
Jones D S 1964 *The Theory of Electromagnetism* (Oxford: Pergamon)
Mason B J 1971 *The Physics of Clouds* (Oxford: Oxford University Press) 2nd edn
Morgan M A and Mei K K (1979) *IEE Trans. Antennas Propag.* **AP 27** 202-14
Ono A 1970 *J. Atmos. Sci.* **27** 649–58
Shepherd J W 1981 *Phd Thesis* University of Essex
Uzunoglu N K, Alexopoulos N G and Fikioris J G 1978 *J. Opt. Soc. Am.* **68** 194–7
Uzunoglu N K, Evans B G and Holt A R 1976 *Electron. Lett.* **12** 312–3
Uzunoglu N K and Holt A R 1977 *J. Phys. A: Math. Gen.* **10** 413–24
Varley D J 1978 *Air Force Geophysics Laboratory Hanscom AFB, Mass, Report AFGL-TR*-78-0792
Waterman P C 1969 *Alta Freq.* **38** (special) 348–52
Watson G N 1966 *The Theory of Bessel Functions* (Cambridge: Cambridge University Press) 2nd edn
Weil H and Chu C-M 1976 *Appl. Opt.* **15** 1832–6
——1980 *Appl. Opt.* **19** 2066–71